Phys. Status Solidi A **208**, No. 9, 2115–2123 (2011) / **DOI** 10.1002/pssa.201026578

physica status solidi a
www.pss-a.com
applications and materials science

Nanometer to micron scale mechanics of [100] silicon nanowires using atomistic simulations at accelerated time steps

Hansung Kim[1] **and Vikas Tomar**[*,2]

[1] Mechanical Engineering Department, Northwestern University, Evanston, IL, 60208, USA
[2] School of Aeronautics and Astronautics, Purdue University, West Lafayette, IN 47907, USA

Received 20 September 2010, revised 19 April 2011, accepted 27 April 2011
Published online 27 May 2011

Keywords atomistic simulations, molecular dynamics, silicon nanowires

[*] Corresponding author: e-mail tomar@purdue.edu, Phone: 765-494-3423, Fax: 765-494-0307

Atomistic simulations have a unique capability to reveal the material deformation mechanisms and the corresponding deformation-based constitutive behavior. However, atomistic simulations are limited by the accessible length and time scales. In the present work an equivalent crystal lattice method is used to perform mechanical deformation atomistic simulations of nanometer to micrometer sized silicon (Si) nanowires at accelerated time steps. The equivalent crystal lattice method's validity is verified by comparing the method's results with the results of classical molecular dynamics (MD) simulations at MD strain rates. The simulations predict that when the nanowire cross-sectional size exceeds 50 nm, the dependence of the nanowire Young's moduli values on the changes in nanowire cross-sectional size is considerably reduced. Analyses show a transition in nanowire failure mechanism from being ductile to being brittle with increase in the nanowire cross-sectional size. Examinations of the surface effect reveal that below a critical surface to volume ratio value of 0.05 nm^{-1}, the peak nanowire strength is independent of further reduction in the surface to volume ratio value. This finding places a size limit on the surface effect observed in Si nanowires.

1 Introduction Silicon (Si) has been the primary material for semiconductor devices since the invention of transistors in the 1940s. Si nanowires are an important technological invention with applicability in new electronic devices, energy generation devices, etc. [1, 2]. Such usage requires mechanistic understanding of the nanowire deformation at the length scales of a few nanometer to a few micrometer. Despite numerous advancements in the processing and the experimental characterization of nanowires, the computational characterization of nanowire mechanical deformation at the length scale of experimentally obtained nanowires has not been performed using atomistic simulations.

In the present work, an advancement in the form of the equivalent crystal lattice method is presented to perform classical atomistic simulations at micron length and seconds time scales. In the equivalent crystal lattice method, the equivalent lattices with lattice constants that are multiples of a material's unit cell crystal lattice are developed while preserving the fractional coordinates, cohesive energy values, elastic constants, defect energy values, and phonon dispersion relations. The equivalent crystal lattice method is used for understanding Si nanowire deformation mechanics up to a length scale of few μmicrometers. The method is integrated in a scalable parallel molecular dynamics (MD) simulation code (DLPOLY) [3]. Nanowire deformation mechanics is an extensively studied field [4]. Due to the vast literature in this field, here the focus is only on reviewing work related to the Si nanowire deformation mechanics. Different simulation methods [*e.g.*, the finite element method (FEM), MD, and *ab initio* methods such as those based on the density functional theory (DFT)] have been used for analyzing the Si nanowire deformation mechanics, *e.g.*, Table 1. Continuum simulations based on FEM require less time and computational effort in comparison to the atomistic simulations. However, the size scale limit at which continuum analyses fail is an important and yet unresolved issue.

Using DFT calculations, Dubois et al. [15] have predicted that at least two shear systems, (111) $<1\bar{2}1>$ and (110) $<1\bar{1}0>$, are responsible for the limitation of ideal strength of Si. Roundy and Cohen [16] have predicted using

Table 1 Properties of single crystal Si nanowire predicted using experiments and simulations (NR: not reported)

		nanowire size (nm)	method	Young's modulus (GPa)	peak stress (GPa)
experiments	Li et al. [5]	74 nm × 510 nm × 50 000 nm	indentation	72 GPa	NR
	San Paulo et al. [6]	120–190 nm (dia) × 8–12 μm	AFM (atomic force microscope)	186 GPa	NR
	Hoffmann et al. [7]	90–190 nm (dia) × 500–2000 nm	AFM	NR	12 (average)
	Tabib-Azar et al. [8]	140 nm (dia) × 10 000 nm	AFM	93 GPa	0.85
		200 nm (dia) × 10 000 nm	AFM	150–250 GPa	0.3–0.56
	Heidelberg et al. [9]	100–200 nm (dia) × unknown length	AFM	158 GPa	NR
	Han et al. [10]	15–70 nm (dia) × unknown length	tension	55–80 GPa	NR
	Li et al. [11]	12–300 nm (thickness) × unknown length	resonant frequency	53–170 GPa	NR
simulation	Kang and Cai [12]	5 (dia) × 50	MD	139	13.2
	Menon et al. [13]	3–4 (dia) × 7.3 tetrahedral	MD	147.3	NR
		3–4 (dia) × 11.2 Cagelike	MD	94.4	NR
	Lee and Rudd [14]	0.61–4 (width) × unknown length	DFT	29.4–122.5	NR
	Hoffmann et al. [7]	90–190 (width) × 500–2000 (length)	FEM		7–18.1

DFT simulations that dislocations may not be visible at low temperature because the entire lattice can become unstable before a dislocation is induced. MD is the most popular tool for analyzing Si nanowire deformation mechanics because of its capability to simulate the behavior of systems with millions of atoms. However, currently it is challenging to use MD to simulate nanowire mechanical deformation when the nanowire diameter is larger than 10 nm and the nanowire length is more than 100 nm at experimentally accessible strain rates ($\sim 10^{-1}$/s) [4].

Two important issues need to be investigated in order to thoroughly understand the deformation mechanics of Si nanowires. First, one should answer what would be the origin of the specimen size effect on mechanical properties; *i.e.*, whether the specimen size effect occurs due to diameter, length, surface area, or other structural effect related to a nanowire specimen. Reported origins of the specimen size effect have been predicted as length [7, 17], diameter [10, 11], surface area [18], and surface roughness [19]. Second, the size limit below which brittle to ductile fracture transition occurs for Si nanowires is not known. Using tensile experiments, Han et al. [10] have reported that the brittle to ductile transition occurs at ~60 nm nanowire diameter. However, brittle to ductile transition has been observed at ~4 nm nanowire diameter during MD simulations [20].

Tremendous research efforts have been directed toward performing atomistic simulations at experimental length and time scales with limited success. Again, due to the vast literature in this field and due to limited space, only a few approaches are cited. One of the most prominent and discussed approach for improving accessible length scale of simulations is the quasi-continuum method [21]. However, this method does not address scaling in time domain. The approaches used for such purpose include utilizing a large number of processors [22], MD temperature acceleration methods [23], and Hybrid Monte Carlo method (HMC) [24]. In the present work, an equivalent crystal lattice framework is used to address this problem. The uniqueness of the method lies in being able to address scaling in length as well as time scale. A choice can be made to scale either one of the time scale and length scale or both.

There are two objectives in this paper. First is to compare the predictions between the equivalent crystal lattice method and classical MD at MD strain rates (since MD strain rates cannot be reduced much without a significant increase in computational cost). Second is to predict the size related mechanical properties of [100] oriented Si nanowires with size in the range of existing experimental measurements. This objective is chosen to understand the capability of method to predict mechanistic information regarding a widely studied problem. The method is specific to Si. Further, for reasons of simplicity, the focus of this research is on only [100] oriented nanowires. The equivalent crystal lattice method can be used to predict results at experimental strain rates. However, in order to compare the method results with the MD simulation results, the present work reports analyses only at MD strain rates.

2 Method and framework

The investigation focuses on analyzing nanowire deformation mechanics with the nanowire diameter ranging from 2.17 nm to 1.74 μm. It is important to note that the equivalent lattices effectively reproduce classical properties. Therefore, the property limitation on MD (such as inability to calculate electronic properties) still applies. In addition, the framework focuses solely on mechanical properties. However, phonon transmission related properties such as thermal conductivity could also be analyzed using the framework.

2.1 Interatomic potential

Si has a diamond cubic crystal structure with the lattice constant value of 5.43 Å. The lattice constants of the equivalent lattices in the present work

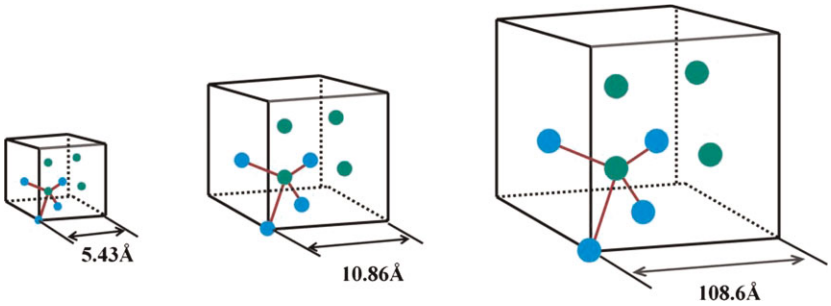

Figure 1 (online color at: www.pss-a.com) An illustration of equivalent crystal lattice unit cells. Blue and green dots are the fractional coordinates of Si atoms. The equivalent lattices preserve the Si crystal structure, albeit with larger lattice constants.

are based on the multiples of Si unit cell lattice constant [10.86 (2×5.43 Å), 108.6, and 1086 Å]. The equivalent lattice unit cells have the same crystal structure as an actual Si unit cell. Figure 1 illustrates this graphically. The well-known potentials for atomistic simulations of Si are Stillinger and Weber (SW) [25], Tersoff (T2 and T3) [26], Dodson (DOD) [27], and Biswas and Hamann (BH) [28] potentials. None of these potentials have been established as the superior. SW, T3, and to some extent DOD are good for simulating elastic properties [29]. T3, SW, DOD, T2, and BH give fairly good values for predicting structures and energetics of intrinsic defects [29]. Only T3 correctly predicts the phase transformation from diamond structure to β-tin phase [29]. Based on these observations, T3 is chosen as the potential form of choice for the equivalent lattices [30, 31]. In this potential, the total atomistic energy E, as a function of atomic coordinates is described as

$$E = \sum_i E_i = \frac{1}{2}\sum_{i \neq j} f_c(r_{ij})\left[f_R(r_{ij}) + b_{ij} f_A(r_{ij})\right]. \quad (1)$$

In the above expression, r_{ij} is the distance between atoms i and j, f_c is an harmonic function of the interatomic distances, f_R is repulsive interaction term, f_A is attractive interaction term, and b_{ij} is a bond order term that depends upon the atomic position of the surrounding atoms j of an atom i. The functions f_c, f_R, and f_A are formulated as,

$$f_R(r) = A^{(-\lambda_1 r)},$$
$$f_A(r) = -B^{(-\lambda_2 r)}, \text{ and}$$
$$f_c(r) = \begin{cases} 1, & r < R-D \\ \frac{1}{2} - \frac{1}{2}\sin\left(\frac{\pi}{2}(r-R)/D\right), & R-D < r < R+D \\ 0, & r > R+D. \end{cases} \quad (2)$$

A detailed information on parameters A, B, R, D, and other parameters mentioned in Table 2 can be found in the work of Tersoff [31]. The inter-atomic potentials of the equivalent lattices are obtained by fitting bulk properties such as cohesive energy values, bulk elastic constants, and lattice constants while maintaining the same fractional coordinates. The bulk modulus as well as the elastic constants of the equivalent crystal lattices should be the same as those of the original crystal lattice (5.43 Å) since those properties are not influenced by the lattice unit cell size. The total lattice energy and atomic mass of an equivalent lattice unit cell should be rescaled in proportion to the volume ratio compared to the original (which will be also called ordinary cell from now on) lattice unit cell. Table 2 lists inter-atomic potential parameters of the equivalent lattices.

Classical molecular simulations use potentials that are fitted to static or experimental properties. Sometimes quantum mechanical datasets are also used. Most of the dataset is either room temperature or at 0 K. In this research dataset for potential fitting is based on experimental measurements that are at room temperature. Since simulations are also performed at room temperature, the temperature does not have any influence on the performed simulations. However, if the simulations were performed at temperatures significantly different from room temperature such as those in the vicinity of 2000 K results would be significantly affected by temperature. This issue is the same as any classical molecular simulations. Classical molecular simulations are limited to the range the interatomic potential can accurately reproduce the properties similar to fitted property dataset.

Table 2 also lists the experimental values of the elastic constants of Si and compares those values with the predictions made by the potentials for different equivalent crystal lattices. The fitting error is within the range of 20% of experimental values which is similar to the error range of the T3. Moreover, cohesive and defect energy values predicted using the interatomic potentials of the equivalent lattices are also compared with those predicted by the original Tersoff potential in Table 2. A maximum error of 11% is observed in the cohesive energy calculations and a maximum error of 13% is observed in the defect energy calculations. These error values are of the same order as predicted using T3.

2.2 Satisfaction of dynamical requirements The next step in ensuring correct prediction of properties using the potentials for the equivalent lattices is that the time step of the atomistic simulations based on the equivalent crystal lattice framework reproduces correct dynamical information. One way to ensure such a reproduction is to ensure that the time steps sufficiently resolve atomic vibration

Table 2 Tersoff empirical potential parameters and predicted properties for equivalent lattices C: elastic constants, B: bulk modulus, E: energy (% error in parenthesis)

			5.43 Å (T3) [26]	10.86 Å (this work)	108.6 Å (this work)	1086 Å (this work)
Tersoff potential parameters	A (eV)		1830.8	2911.8	9682.2728	12 256.2453586
	B (eV)		471.18	1500	2500.0	28 469.546054
	λ_1 (Å^{-1})		2.4799	0.2125	0.4195	0.04235
	λ_2 (Å^{-1})		1.7322	1.8166	1.08071	0.008282
	α		0	0	0	0
	n		0.78734	0.78734	0.78734	0.78734
	β		1.0999×10^{-6}	1.0699×10^{-6}	1.0699×10^{-6}	1.0699×10^{-6}
	n		0.78734	0.78734	0.78734	0.78734
	c		100390	100390	100390	100 390
	d		16.218	16.418	16.418	16.418
	h		−0.59826	−0.59826	−0.59826	−0.59826
predicted properties	C_{11} (GPa) fitting target: 165.7 [32]		142.5 (14)	137.0 (17)	134.86 (18.6)	136.6 (17.5)
	C_{12} (GPa) fitting target: 63.9 [32]		75.4 (18)	70.0 (9.7)	68.13 (6.63)	73.5 (15)
	C_{44} (GPa) fitting target:79.6 [32]		69 (13.3)	67.42 (15)	67 (15.8)	64.8 (18.6)
	B (GPa) fitting target: 98 [33]		98 (0.0)	98.5 (0.6)	90.37(7.7)	94.5 (3.5)
	lattice E (eV) fitting target: −37.36 [33]		−37.04(0.9)	−36.175 (0.14)	−37.29 (0.1)	−37.3(0.05)
	predicted vacancy E (eV)		3.7	3.4	3.5	3.7
	predicted interstitial E (tetrahedral, eV)		3.8	3.3	3.7	3.9
	predicted cohesive E (eV)	diamond	−4.63	−4.52	−4.66	−4.67
		simple cubic	−4.31	−4.42	−4.54	−4.53
		face center cubic	−3.87	−4.30	−4.38	−4.41
		body center cubic	−4.20	−4.40	−4.49	−4.53

frequencies for the equivalent crystal lattices. In order to satisfy the conservation of mass requirement, the atomic mass in the equivalent lattices is scaled as the lattice constants are scaled up. This is expected to change the phonon dispersion curves for the new lattices. In order to examine this issue, phonon dispersion relations (first four acoustic branches) corresponding to all three lattices examined in this research are plotted in Fig. 2. As shown, all the phonon dispersion relations have the same shape. The frequency magnitudes, however, are scaled down in accordance with the scaling magnitude of the lattice constant. For 2 times scaling of the lattice constant,

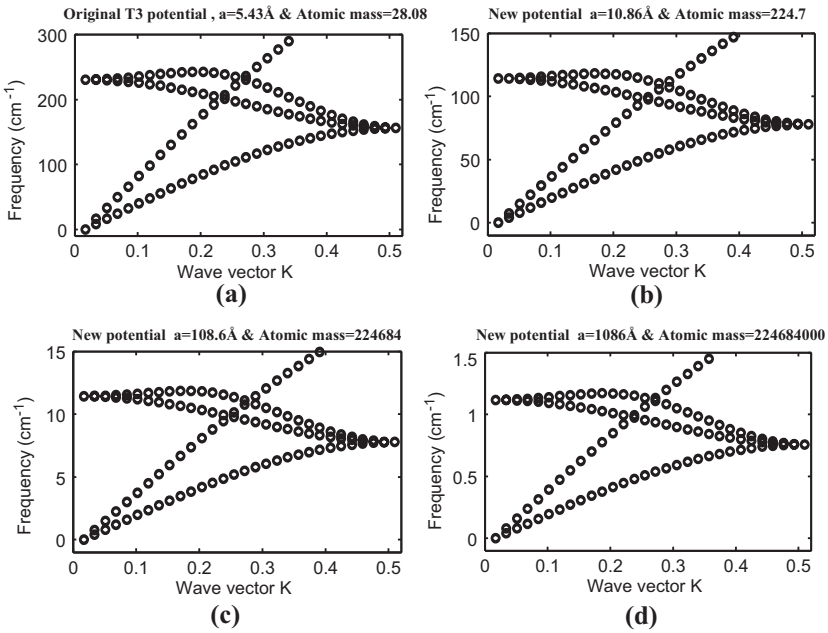

Figure 2 Phonon dispersion relations for (a) original Si crystal lattices, (b) crystal lattice scaled 2 times, (c) crystal lattice scaled 20 times, and (d) crystal lattice scaled 200 times.

frequency magnitudes are reduced by ½. For 20 times scaling, the frequency magnitudes are reduced by 1/20th. We have examined phonon dispersion relations for higher frequency braches as well. The trend observed (not shown here for clarity) is repeated in the exact same manner.

Since frequencies reduce in a manner directly proportional to the increase in the lattice constant values, it can be concluded that the maximum MD time step should increase in a directly proportional manner as well. The scaled up time step values based on this criterion can further be modified by considering two practical issues: (1) time step should be such that atoms are constrained to move not more than 1/20th of the nearest-neighbor distance at five times the maximum thermal velocity among all atoms in a system; and (2) time step should be such that atoms are constrained to move not more than 1/20th of the nearest neighbor distance at the maximum absolute velocity among all atoms in a system [34].

One also needs to address additional considerations before finalizing the maximum time step with equivalent crystal lattices. Namely, we need to satisfy the requirement of ergodicity as well as stability of NPT (grand canonical ensemble), NVE (microcanonical ensemble), and NVT (canonical ensemble) equations of motions [35]. Final time steps of choice after taking into account all of the above considerations were 0.5 ps for 1086 Å lattice constant, 0.05 ps for 108.6 Å lattice constant, and 0.005 ps for 10.86 Å lattice constant.

2.3 Simulation details All the reported simulations are performed at 300 K. In order to control the temperature and stress, Nose'-Hoover thermostat and barostat are used. Constant stress $N\sigma T$ ensemble (constant number of particles, stress, and temperature) is used for statistical thermodynamic description. The strain rate is of the order of $10^8\ s^{-1}$ in all the simulations in order to provide a common ground of comparison with the MD and the equivalent crystal method results. Velocity Verlet integration algorithm is used for integrating classical equations of motion. Visual MD (VMD) [36] software is used for the visualization of the atomic deformation. Three different types of nanowire supercell are constructed corresponding to each equivalent lattice, Table 3. Along the lateral nanowire supercell surfaces enough gap is provided (calculated based on cutoff radius) so that the nanowires examined have free surfaces. The smallest dimension of the nanowire is 2.17 nm × 2.17 nm × 17.36 nm, which is based on the 5.43 Å Si lattice. The dimension increases to 1.74 μm × 1.74 μm × 3.48 μm when 1086 Å equivalent lattice is employed.

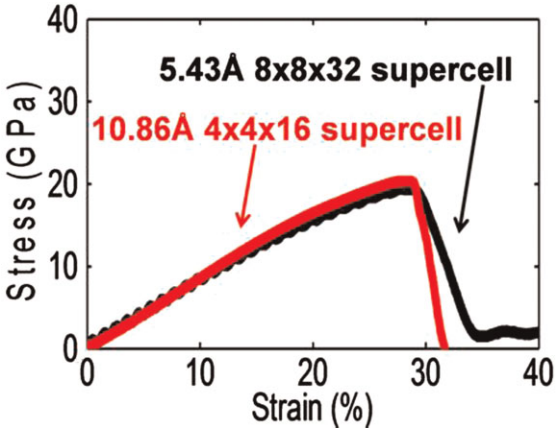

Figure 3 (online color at: www.pss-a.com) Stress *versus* strain curve for 4 × 4 × 16 lattice constant supercell of 10.86 Å lattice and 8 × 8 × 32 lattice constant supercell of 5.43 Å lattice. The dimension is 4.34 nm × 4.34 nm × 17.36 nm for both nanowires.

3 Results Before proceeding with the equivalent crystal lattice method-based analyses, the MD predictions of stress–strain curves for an 8 × 8 × 32 supercell nanowire made up of original Si crystal lattice atoms were compared with the predictions of stress–strain curves for a 4 × 4 × 16 supercell nanowire made up of 10.86 Å equivalent crystal lattice atoms, Fig. 3. This supercell choice results in the nanowires with exactly the same sizes. As shown, the agreement in Young's moduli value prediction between the two supercells is within 1% error and the agreement in peak stress prediction is within 1.5% error. In the case of nanowires made up of equivalent lattices with lattice constants of 108.6 and 1086 Å, a direct comparison with the results for a corresponding nanowire made up of 5.43 Å lattice constant Si atoms is not achievable because of the computational infeasibility of simulating billions of atoms at infeasible strain rates necessary for such comparison. However, as shown later, the stress–strain curves of the nanowires with unit cells of larger lattice constants correspond closely to those of the nanowires made up of 5.43 Å lattice constant and 10.86 Å lattice constant unit cells.

Figure 4 shows a comparison of the fracture mechanism between the 8 × 8 × 32 supercell nanowire made up of original Si crystal lattice atoms and the 4 × 4 × 16 supercell

Table 3 Description of atomistic supercells of nanowires for simulations

supercell size	5.43 Å lattice constant	10.86 Å lattice constant	108.6 Å lattice constant	1086 Å lattice constant
4 × 4 × 32	2.17 nm × 2.1 nm7 × 17.36 nm (4096 atoms)	4.34 nm × 4.3 nm4 × 34.8 nm (4096 atoms)	43 nm × 43 nm × 348 nm (4096 atoms)	0.43 μm × 0.43 μm × 3.48 μm (4096 atoms)
8 × 8 × 32	4.34 nm × 4.3 nm4 × 17.36 nm (16 384 atoms)	8.7 nm × 8.7 nm × 34.8 nm (16 384 atoms)	87 nm × 87 nm × 348 nm (16 384 atoms)	0.87 μm × 0.87 μm × 3.48 μm 16 384 atoms)
16 × 16 × 32	8.7 nm × 8.7 nm × 17.36 nm (65 536 atoms)	17.4 nm × 17.4 nm × 34.8 nm (65 536 atoms)	174 nm × 174 nm × 348 nm (65 536 atoms)	1.74 μm × 1.74 μm × 348 μm (65 536 atoms)

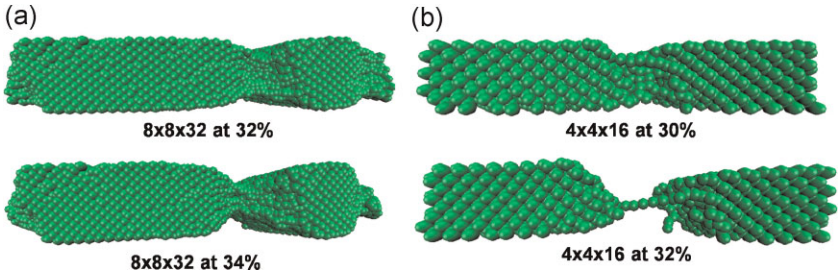

Figure 4 (online color at: www.pss-a.com) Comparison of fracture behavior between (a) $8 \times 8 \times 32$ lattice constant supercell nanowire based on 5.43 Å lattice and (b) $4 \times 4 \times 16$ lattice constant supercell nanowire based on 10.86 Å equivalent lattice. The supercell choices correspond to nanowires with exactly the same sizes.

nanowire made up of 10.86 Å equivalent crystal lattice atoms. As shown, both the MD and the equivalent crystal lattice method predict same fracture initiation location and fracture strain. The fracture separation occurred in ductile fashion. Prior to separation, crystalline to amorphous structural transition was observed in regions near the fracture surfaces. This mechanism has been reported in the experiments by Han et al. [10] as well as in the simulations by Menon et al. [13]. In almost all cases, the failure initiated at the nanowire surfaces. Sometimes, multiple failure-initiation points are observed on the surfaces.

3.1 Fracture mechanism Figure 5 shows stress–strain plots for all nanowires. As claimed earlier, stress–strain curves for all the nanowires correspond closely till the peak-stress point. The corresponding peak strain falls within a close range for all the nanowires. A detailed analysis of the plots in Fig. 5 will be presented in the discussion section. One important issue to be noticed is that tensile strength is increasing with increase in lattice size. Widely observed and discussed surface to volume ratio is behind such effect [18]. It is well documented that higher the ratio less is the tensile strength. With scaling in lattice constant values the surface to volume reduces leading to increase in the tensile strength. Using MD simulations, it has been observed that [110] nanowires with diameters less than 4 nm fail by ductile fracture even at room temperature while thicker nanowires fail by brittle fracture mechanism [20]. Through tensile experiments, Han et al. have reported brittle to ductile transition occurred around 60 nm diameter for [110] Si nanowires [10].

During simulations, the ductile to brittle transition in fracture of Si nanowires was also observed, Fig. 6. Figure 6(a) illustrates the fracture behavior of 8.7 nm × 8.7 nm × 17.36 nm Si nanowire, which clearly shows the ductile fracture mechanism. Figure 6(b) illustrates the fracture behavior of 17.4 nm × 17.4 nm × 34.8 nm Si nanowire with Si lattice with two times lattice constant (65536 atoms), which clearly shows the brittle fracture mechanism. Figure 6(c) illustrates the fracture behavior of 17.4 nm × 17.4 nm × 34.8 nm Si nanowire made up of original Si crystal lattice showing that the fracture mechanism is not affected by replacing MD with the equivalent crystal lattice method. The fracture surface examinations in the case of Fig. 6(b) and (c) revealed that the final separation is preceded by amorphization at the fracture location. This observation agrees with the experimental and computational observations made by other researchers and groups. Discrepancy in the simulation predictions and experimental predictions can be attributed to (1) the nanowire orientation being different from the earlier experiments and calculations and (2) the nanowires not being the exact same shape as examined in the experiments.

4 Discussions

4.1 Effect of specimen size on the peak stress of Si nanowires During analyses of the specimen size effect in Si nanowires, either nanowire diameter or nanowire length has been used as the most influencing variable that affects nanowire strength. Researchers have also noticed that a large surface to volume ratio in the case of nanowires is responsible for the nanowire mechanical properties being

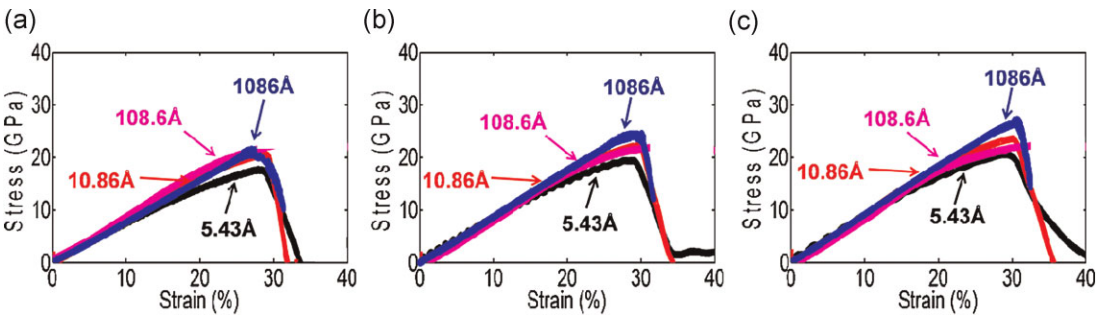

Figure 5 (online color at: www.pss-a.com) Stress–strain curve comparison for (a) $4 \times 4 \times 32$ lattice constant supercell nanowires with all lattice constants, (b) $8 \times 8 \times 32$ lattice constant supercell nanowires with all lattice constants, (c) $16 \times 16 \times 32$ lattice constant supercell nanowires with all lattice constants.

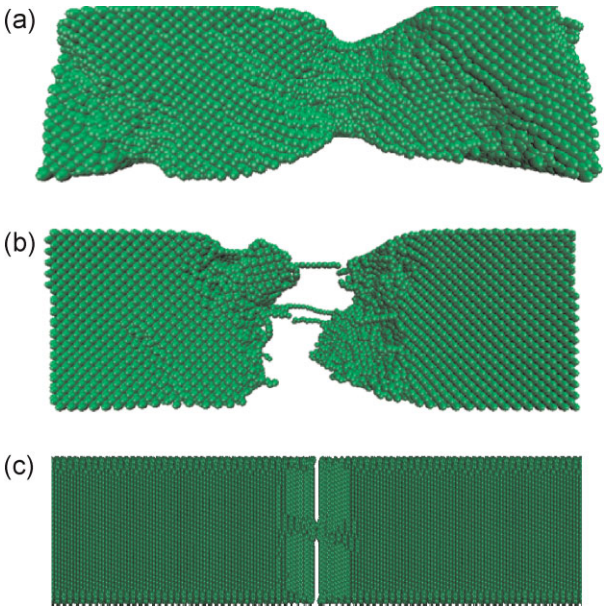

Figure 6 (online color at: www.pss-a.com) Ductile and brittle fracture mechanisms, respectively, in the cases of (a) 8.7 nm × 8.7 nm × 17.36 nm Si nanowire with original Si lattice (65 536 atoms), (b) 17.4 nm × 17.4 nm × 34.8 nm Si nanowire with Si lattice with two times lattice constant (65 536 atoms), and (c) 17.4 nm × 17.4 nm × 34.8 nm Si nanowire with original Si lattice (524 288 atoms).

different from the bulk counterparts. However, the critical value of surface to volume ratio at which the effect of surface on nanowire strength vanishes has not been examined. To analyze the effect of surface to volume ratio on the nanowire mechanical properties, the peak stress values are plotted as a function of the surface to volume ratio in Fig. 7. Since multiple samples correspond to the same surface to volume ratio, Fig. 7 also shows error bar. As shown, the error bar is unaffected by the change in values of surface to volume ratio.

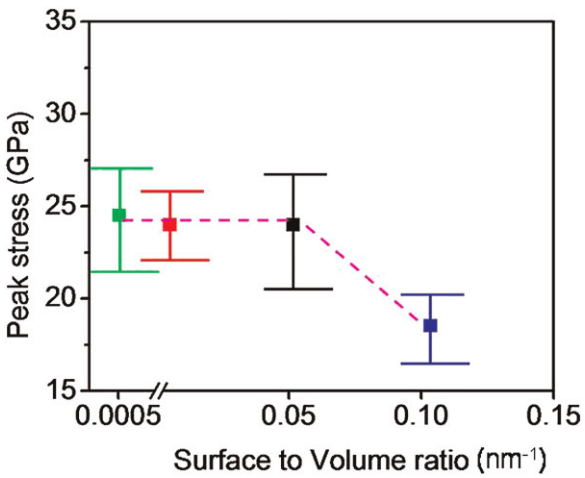

Figure 7 (online color at: www.pss-a.com) Peak stress as a function of surface to volume ratio.

However, the peak stress values become independent of the surface to volume ratio at the ratio values lower than 0.05 nm^{-1}. The peak stress values converge to a value in the vicinity of 25 GPa. It is well documented that the nanowires' surfaces act as defect nucleation sites. With increase in the surface to volume ratio, the available surface area increases. This directly leads to a higher extent of defect formation and the corresponding lowering of peak stress values leading to nanowire softening. When compared to the experimental peak stresses shown earlier in Table 1, the peak stress predicted in MD and equivalent crystal lattice simulations are higher than those predicted in experiments. The reason for the higher stress is partly the high effective strain rate of current simulations and partly the absence of initial defects in the simulated supercells. Experimental measurements are at lower strain rates and, possibly, in the presence of defects (based on discussions with Si nanowire growers).

4.2 Effect of specimen size on Young's modulus of Si nanowires The transition diameter, as discussed in the nanowire mechanics literature, is the maximum nanowire diameter (in the case of present work it is denoted by the characteristic cross-sectional size which is the diameter of a circle that confines the square cross-section of a simulated nanowire) beyond which the nanowire Young's modulus value approaches the corresponding bulk value of the nanowire material. Since the reported simulations employed nanowires with diameter approaching 150 nm, the predicted Young's moduli can be used to obtain a trend on the transition diameter. Size limited MD simulations by different researchers have reported different transition diameter values for Si nanowires ranging from 4 to 30 nm (mostly less than 10 nm). Figure 8 shows the Young's moduli values for Si nanowires predicted by different researchers as a function of nanowire diameter. A dotted line is drawn to form a two-part least square fit to the experimental data. The fit is a good approximation to the overall data with the exception of data by Ref. [10]. It is to be noted that experiments used different Si nanowire

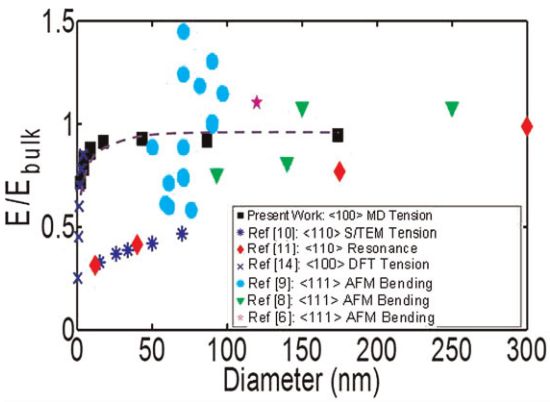

Figure 8 (online color at: www.pss-a.com) A comparison of Young's moduli predictions as a function of Si nanowire diameter in experiments and in current simulations.

growing methods resulting in nanowires with different surface roughness and varied texture. Therefore, an exact fit between simulations and experiments is not likely.

As shown in Fig. 8, the results of present work closely approximate a two-part least square fit. It is clear that the experimental value of transition diameter in the case of Si exceeds 50 nm. Previous experiments have conjectured that the transition diameter should lie in the vicinity of 100 nm [4, 9, 11]. The simulation results (black filled squares) closely approximate the experimental trend. As the nanowire cross-sectional size exceeds 50 nm, the Young's moduli values are not affected by the variation in the cross-section size. As discussed earlier, the present work shows for the first time that a critical value of surface to volume ratio exists below which surface effect vanishes. It is clear from Fig. 8 that the critical value of surface to volume ratio corresponds to a transition diameter value of at least 50 nm beyond which the Young's moduli are not affected by the nanowire surface to volume ratio.

4.3 A perspective on using equivalent lattices for speeding-up atomistic simulations The essence of the equivalent crystal method lies in producing equivalent lattices that have the same crystal structure as that of the original lattice but have larger lattice constant. As shown earlier conservation of mass, momentum, and energy is ensured during simulations. Also, as shown earlier defect energy values of the equivalent crystals are the same as those predicted for the original lattices. MD is a classical approach and the equivalent crystal method replicates MD at higher length scale and time scale in much the same essence as MD is performed. Therefore, method has the same limitations as those of MD. However, the method is able to perform the calculations performed by MD at much higher length and time scales. MD, itself, is not great in predicting bond failure which leads to fracture. Majority of defects nucleate at atomistic length scales. In that sense the equivalent crystal method which is performed at higher length scale cannot be used to understand the nucleation of defects. However, being performed at higher length and time scale the equivalent crystal method can be used to understand the propagation of defects atomistically at higher length and time scales than MD.

MD is still applicable at the length scale of its application. In the method when equivalent crystals are replaced by actual unit cells the method actually is the same as MD. MD can be used to understand the formation of defects, and an understanding of mechanisms at time scale and length scales upto few nanoseconds and nanometers, respectively. For higher length scales and time scales one can use scaled up lattices in the equivalent crystal lattice method. Like MD, the equivalent crystal method based simulations can be performed at specified finite temperature values.

At the beginning of Section 3, tensile deformation behavior of two Si nanowire supercells was compared: the first supercell with 5.43 Å lattice constant and the second supercell with 10.86 Å lattice constant. The supercells had the same overall dimension of $4.43\,\text{nm} \times 4.43\,\text{nm} \times 17.36\,\text{nm}$. Using the equivalent lattice with 10.86 Å lattice constant instead of the original Si lattice with 5.43 Å lattice constant, the number of atoms required to construct a supercell of $4.43\,\text{nm} \times 4.43\,\text{nm} \times 17.36\,\text{nm}$ dimension is reduced by approximately eight times (16 384 atoms *vs*. 2048 atoms). At the same time, such replacement enabled an increase in the simulation time step by five times (5 fs vs. 1 fs). Correspondingly, the overall computational time was reduced by approximately ten times (0.29 s/time step *vs*. 0.03 s/time step). Since the equivalent lattice method scales both in length and time scales, a significant reduction in computing time can be achieved when this method is employed.

5 Conclusions Atomistic simulations of Si nanowires are performed using an equivalent crystal lattice method. The method replaces original Si crystal lattices with larger-scale exact replicas (called equivalent lattices) that have the same dynamical properties as approximated by the Tersoff potential for the original Si crystal lattice. The method's results agree well with both the MD simulations and the experiments. The use of the equivalent lattices increased the atomistic simulation time step by an order of 500. The approach is implementable in standard MD codes (DLPOLY in this case). It is shown that using the method, it is possible to simulate nanowires with cross-section size ranging from nanometers to micrometers. The presented analyses have shown a seamless transition from the classical MD atomistic scale results to continuum scale experimental results in Si nanowire deformation mechanics.

Using the method, atomistic simulations of [100] oriented Si nanowire deformation with diameter approaching 1.74 μm were performed for the first time. New findings related to the effect of surfaces on nanowire Young's moduli and peak stress values were reported. The dynamical deformation analyses predict that the nanowire Young's moduli values approach bulk values when cross-sectional size exceeds 50 nm. Analyses also predict a transition in failure mechanism from being ductile to being brittle with an increase in nanowire cross-sectional size. It is shown that when the nanowire surface to volume ratio value approaches 0.05, the surface effect on the nanowire peak strength vanishes.

UNCLAS: Dist. A. Approved for public release.

References

[1] D. R. Khanal, J. W. L. Yim, W. Walukiewicz, and J. Wu, Nano Lett. **7**, 1186 (2007).
[2] X. Y. Wu, J. S. Kulkarni, G. Collins, N. Petkov, D. Almecija, J. J. Boland, D. Erts, and J. D. Holmes, Chem. Mater. **20**, 5954 (2008).
[3] W. Smith, C. W. Yong, and P. M. Rodger, Mol. Simul. **28**, 385 (2002).
[4] C.-H. Cho, S.-K. Kim, B.-H. Kim, and S.-J. Park, Appl. Phys. Lett. **95**, 243108 (2009).

[5] B. Li, M. K. Kang, K. Lu, R. Huang, P. S. Ho, R. A. Allen, and M. W. Cresswell, Nano Lett. **8**, 92 (2008).
[6] A. San Paulo, J. Bokor, R. T. Howe, R. He, P. Yang, D. Gao, C. Carraro, and R. Maboudian, Appl. Phys. Lett. **87**, 3 (2005).
[7] S. Hoffmann, I. Utke, B. Moser, J. Michler, S. Christiansen, V. Schmid, S. Senz, P. Werner, U. Gosele, and C. Ballif, Nano Lett. **6**, 622 (2006).
[8] M. Tabib-Azar, M. Nassirou, R. Wang, S. Sharma, T. I. Kamins, M. S. Islam, and R. S. Williams, Appl. Phys. Lett. **87**, 3 (2005).
[9] A. Heidelberg, L. T. Ngo, B. Wu, M. A. Phillips, S. Sharma, T. I. Kamins, J. E. Sader, and J. J. Boland, Nano Lett. **6**, 1101 (2006).
[10] X. D. Han, K. Zheng, Y. F. Zhang, X. N. Zhang, Z. Zhang, and Z. L. Wang, Adv. Mater. **19**, 2112 (2007).
[11] X. X. Li, T. Ono, Y. L. Wang, and M. Esashi, Appl. Phys. Lett. **83**, 3081 (2003).
[12] K. Kang and W. Cai, Philos. Mag. **87**, 2169 (2007).
[13] L. Menon, S. Patibandla, K. Bhargava Ram, S. I. Shkuratov, D. Aurangzeb, M. Holtz, J. Berg, J. Yun, and H. Temkin, Appl. Phys. Lett. **84**, 4735 (2004).
[14] B. Lee and R. E. Rudd, Phys. Rev. B **75**, 13 (2007).
[15] S. M. M. Dubois, G. M. Rignanese, T. Pardoen, and J. C. Charlier, Phys. Rev. B **74**, 7 (2006).
[16] D. Roundy and M. Cohen, Phys. Rev. B **64**, 212103 (2001).
[17] T. Tsuchiya, O. Tabata, J. Sakata, and T. Yasunori, J. Microelectromech. Syst. **7**, 106 (1998).
[18] W. N. Sharpe, K. M. Jackson, K. J. Hemker, and Z. L. Xie, J. Microelectromech. Syst. **10**, 317 (2001).
[19] T. Namazu, Y. Isono, and T. Tanaka, J. Microelectromech. Syst. **9**, 450 (2000).
[20] K. Kang and W. Cai, Int. J. Plasticity **26**, 1387 (2010).
[21] E. B. Tadmor, R. Philips, and M. Ortiz, Philos. Mag. A **73**, 1529 (1996).
[22] T. C. Germann and K. Kadau, Int. J. Mod. Phys. C **19**, 1315 (2008).
[23] A. F. Voter, F. Montalenti, and T. C. Germann, Annu. Rev. Mater. Res. **32**, 321 (2002).
[24] V. Tomar, J. Appl. Phys. **101**, 103512 (2007).
[25] F. H. Stillinger and T. A. Weber, Phys. Rev. B **31**, 5262 (1985).
[26] J. Tersoff, Phys. Rev. B **38**, 9902 (1988).
[27] B. W. Dodson, Phys. Rev. B **35**, 2795 (1987).
[28] R. Biswas and D. R. Hamann, Phys. Rev. Lett. **55**, 2001 (1985).
[29] H. Balamane, T. Halicioglu, and W. A. Tiller, Phys. Rev. B **46**, 2250 (1992).
[30] J. Tersoff, Phys. Rev. B (Rapid Commun.) **39**, 5566 (1989).
[31] J. Tersoff, Phys. Rev. Lett. **56**, 632 (1986).
[32] H. J. McSkimin and P. Andreatch, J. Appl. Phys. **35**, 2161 (1964).
[33] M. T. Yin and M. L. Cohen, Phys. Rev. B **26**, 5668 (1982).
[34] K. Nordlund, http://beam.acclab.helsinki.fi/∼knordlun/atomistiset/ (2003).
[35] V. Tomar, Phys. Status Solidi A **204**, 3340 (2007).
[36] W. Humphrey, A. Dalke, and K. Schulten, J. Mol. Graphics **14**, 33 (1996).